Electronic Supplementary Material

Deciphering the intermolecular interactions for separating bicyclic and tricyclic aromatics via different naphthalene-based solvents

Pengzhi Bei[1], Antony Rajendran[2], Jie Feng[1], Wen-Ying Li (✉)[1]

1 State Key Laboratory of Clean and Efficient Coal Utilization, Taiyuan University of Technology, Taiyuan 030024, China

2 Department of Chemistry, Mepco Schlenk Engineering College (Autonomous), Sivakasi 626005, India

E-mail: ying@tyut.edu.cn

Experimental section

A1 Chemical reagents

The chemical reagents used in this work have been listed in Table S1. All the chemical reagents have been purified under a vacuum in a desiccator at 80 ℃ over 12 hrs.

A2 Preparation methods of separation samples

Model compound: naphthalene and phenanthrene have been selected as typical compounds of bicyclic and tricyclic aromatic hydrocarbons to study, respectively, because the concentrations of naphthalene and phenanthrene are higher in bicyclic and tricyclic aromatic hydrocarbons. According to the concentration of bicyclic and tricyclic aromatic hydrocarbons in coal tar, the

naphthalene and phenanthrene mixture has been prepared with a mass ratio of 1:1 as a model compound. Both naphthalene and phenanthrene were dissolved in dichloromethane. Then, dichloromethane was removed under heating in the rotary evaporator to get the naphthalene-phenanthrene mixture. Moreover, to comprehensively investigate the separation performance in real conditions, real coal tar was chosen for further research.

A3 Procedure for separation and regeneration

Different naphthalene-based solvents were prepared in advance as shown in Table S1. Ethylene glycol was stirred with different types of naphthalene-based compounds to form mixed solvents at 50 ℃ for 50 min, where the molar fraction of naphthalene-based compounds varied from 2 to 12 mol%. Thus, the naphthalene-based solvent mentioned in this work refers to the mixture of naphthalene-based compounds and ethylene glycol. The specific separation experiments were performed as follows: First, the prepared naphthalene-phenanthrene mixture was added to the solvents and stirred at different temperatures. The obtained mixture was filtered to obtain a filter cake and filtrate. Then, n-hexane was added to the filtrate obtained in the first step. Afterward, the precipitated solid was filtered and the resultant filtrate was distilled under reduced pressure to recover n-hexane. The separation coefficient (*K*), purity, and yield were calculated to compare the separation performance of different types of naphthalene-based solvents according to the equations given below.

$$K_i = \frac{C_i^f}{C_i^c} \quad ; \quad Purity = \frac{C_i^c}{C_j}; \quad Yield = \frac{m_s C_i^c}{m_0}$$

where， C_i^f and C_i^c denote the concentrations of naphthalene or phenanthrene in the filtrate and filter cake, respectively. *K* represents the partition coefficient of phenanthrene or naphthalene, and *i*

denote phenanthrene or naphthalene. C_j represents the concentrations of the initial compound. m_s and m_0 denote the mass of separated and initial samples.

The back-extraction process was performed using n-hexane as an anti-solvent. The amount of used n-hexane was 3 times that of filtrate. Back-extraction solvent was gradually added into the filtrate, and the mixture has been stirred for 60 minutes at room temperature. Afterwards, these two phases were separated. Finally, the compound in n-hexane was recovered by vacuum distillation. The solvent regenerated by this method can be reused.

A4 Analytical methods

The composition analysis of real coal tar and the separated products was performed by GC×GC-MS (QP2020, Japan) equipped with a flame ionization detector. Helium was used as the carrier gas at a 1.0 mL/min flow rate. The injection volume was 1 μL, and the split ratio was 5:1. The mass spectrometer detection conditions were the temperature of 280 ^{o}C, and 70 eV emission voltages. The modulation period was 5 seconds.

The contents of naphthalene and phenanthrene and the differences in intermolecular interactions between naphthalene-based solvents and naphthalene/phenanthrene were analyzed using ultraviolet–visible spectrometer (CARY 300, USA). The absorption peaks of phenanthrene at 250 nm and naphthalene at 220 nm do not overlap as shown in Figure S1, and the degree of distinction is apparent. Therefore, 250 and 220 nm are the characteristic peaks of phenanthrene and anthracene, respectively. Meanwhile, the interaction between naphthalene-based solvents and naphthalene or phenanthrene has been verified.

The functional groups of regenerated solvents were investigated by Fourier transform infrared

(FT-IR) spectrometer (NEXUS-470, USA) at a wavenumber range from 400 to 4000 cm^{-1}.

A5 Determination of separation mechanism

The simulations were meticulously conducted using the Gaussian 09 program package [1,2]. The geometry optimizations for each compound were executed utilizing the M06-2X method, paired with the 6-311+G(d,p) basis set. This combination was selected for its proven effectiveness in accurately predicting molecular structures and energies. For structures presenting complex conformations, we performed frequency analyses at the M06-2X/6-311+G(d,p) level. This step was crucial to confirm that the optimized geometries corresponded to true minima, as evidenced by the absence of imaginary frequencies. To ensure the comprehensiveness of our optimization process, we initiated the procedure with more than three distinct geometries for each compound. The geometry exhibiting the lowest energy was subsequently identified as the global minimum, serving as the foundation for further analyses. Building on this groundwork, single-point energy calculations were conducted on the optimized geometries, employing the M06-2X/6-311++G(d,p) level. This advanced level of theory provided a more accurate depiction of energies, critical for our study's objectives. Following the optimization, we engaged in various simulation calculations based on the derived geometries, facilitating a deep dive into the molecular behaviors and properties under investigation. For the purpose of conducting an energy decomposition analysis [3], molecular files for various compounds are generated subsequent to the optimization of the substances. These files serve as the foundational input for the current system, which are then processed using Multiwfn program. The final step involves directing Multiwfn to the dedicated energy decomposition analysis folder, facilitating a detailed examination of the diverse interaction energies present within the

mixtures. In the workflow of localized orbital locator (LOL) analysis [4], the first step entails the acquisition of the optimized molecular file, which is then promptly loaded into the Multiwfn software suite. A critical examination of the molecular orbitals is essential at this juncture, with a concerted effort to precisely identify the π orbitals utilized by the molecule. This task includes documenting the positions of atoms integral to these π orbitals, alongside a thorough shield of orbitals beyond the π orbital. Subsequently, an optimal plane must be judiciously selected to facilitate the crafting of LOL-π maps for the molecule in question. This phase is instrumental in vividly illustrating the electron distribution patterns within the π orbitals, thereby shedding light on the molecule's electronic architecture and its consequent different properties. In conducting a reduced density gradient (RDG) analysis [5], one initiates the process by importing the optimized molecular file into the Multiwfn software. This step is followed by the generation of the requisite grid data file, laying the groundwork for the analysis. Subsequent to this, the selection of the appropriate horizontal and vertical axes, along with the determination of the desired quality level, facilitates the acquisition of scatter plot data. The culminating step involves the creation of RDG color-filled scatter maps, employing advanced plotting tools. This methodical approach allows for a nuanced exploration of non-covalent interactions within the molecular framework, providing invaluable insights into the molecule's stability and reactivity patterns. In conducting independent gradient model (IGM) analysis, the initial step requires activating the IGM module within Multiwfn program, following the integration of the optimized molecular file [6,7]. This analytical phase is critical for dissecting the intermolecular interactions with precision. The methodology involves segmenting the molecule into distinct fragments and selecting a simulation quality level that aligns with the objectives of the analysis, thereby optimizing the accuracy of the results. The software then

proceeds to generate an output file reflective of these configurations. Subsequently, this output is imported into VMD, facilitating the generation of an IGM visualization. This step is paramount in providing a comprehensive depiction of the intermolecular forces at play, thus offering invaluable insights into the intermolecular interaction. In the assessment of electron density differentials, the Multiwfn program stands at the forefront, facilitating the precise execution of subtraction operations on wave function files from distinct molecular entities. This methodological step is pivotal, enabling the derivation of the electron density difference function, a fundamental measure reflecting electronic redistribution phenomena associated with molecular interactions or transformations. Adjustments to the grid data quality level are meticulously made to optimize the fidelity and resolution of the analytical output. Subsequently, this refined dataset is imported into the VMD platform, where it undergoes visualization processes that culminate in the production of high-definition images. The wave function was analyzed using the program Multiwfn, and all the isosurfaces were described using VMD [8,9].

Table S1. Details of the chemical reagents used in this work

Chemicals reagents	Purity/wt%	Source
ethylene glycol	99	Shanghai Aladdin Biochemical Co., Ltd
naphthylacetonitrile	98	Shanghai Aladdin Biochemical Co., Ltd
naphthylacetic acid	96	Shanghai Aladdin Biochemical Co., Ltd
naphthaleneacetamide	98	Shanghai Macklin Biochemical Technology Co., Ltd
naphthalenemethanol	99	Shanghai Aladdin Biochemical Co., Ltd
naphthylamine	99	Shanghai Macklin Biochemical Technology Co., Ltd
naphthaleneethanol	98	Shanghai Macklin Biochemical Technology Co., Ltd
naphthol	96	Shanghai Aladdin Biochemical Co., Ltd
n-hexane	99	Tianjin Kemiou Chemical Reagent Co., Ltd
naphthalene	97	Shanghai Macklin Biochemical Technology Co., Ltd
phenanthrene	97	Shanghai Macklin Biochemical Technology Co., Ltd

Table S2 Detailed composition analysis of coal tar

Serial number	Residence time/min	Volume percentage/%	Library ID
1	13.6719	0.0812	flavone, 5,7-dihydroxy-6c-glucoside
2	14.0779	0.1583	corynan-17-ol, 18,19-didehydro-10-methoxy-
3	14.1808	0.1386	2H-benzazepine-2-carboxylic acid, 1,3,4,5-tetrahydro-5-methyl-1-oxo-3-spirocyclohexane-, methyl ester
4	14.2829	0.1126	corynan-17-ol, 18,19-didehydro-10-methoxy-
5	14.4847	0.3405	colchicine
6	14.5886	6.0579	naphthalene
7	14.6964	0.5569	corynan-17-ol, 18,19-didehydro-10-methoxy-
8	14.9009	0.0344	endrin
9	15.1292	0.0531	silane, trichlorodocosyl-
10	15.3363	0.4944	1,2,3,4-tetrahydroisoquinolin, 2-acetyl-6,7-dimethoxy-1-phenmethylene-
11	15.4385	0.0444	dasycarpidan-1-methanol, acetate (ester)
12	15.8412	0.9488	gibberellic acid
13	16.1453	0.0481	cyclotrisiloxane, hexamethyl-
14	16.6511	0.8897	5H-Cyclopropa[3,4]benz[1,2-E]azulen-5-one, 9a-(acetyloxy)-3-[(acetyloxy)methyl]-1,1a,1b,4,4a,7a,7b,8,9,9a-decahydro-7b,9-dihydroxy-1,1,6,8-tetramethyl-, [1ar-(1aα,1bß,4aα,7aα,7bα,8α,9ß,9aα)]-
15	16.8538	0.8307	1,2,3,4-Tetrahydroisoquinolin, 2-acetyl-6,7-dimethoxy-1-phenmethylene-
16	16.9551	0.5511	corynan-17-ol, 18,19-didehydro-10-methoxy-
17	17.2613	0.2883	sumatriptan
18	17.3662	0.7523	ruthenium, tricarbonyl[(3,4)-4,5-diethyl-2,2-dimethyl-3-(1-methylethenyl)-1-thia-2-sila-5-boracyclopent-3-ene]-
19	17.4732	0.3537	corynan-17-ol, 18,19-didehydro-10-methoxy-
20	17.5761	0.2223	5,8,11-eicosatriynoic acid, TMS derivative
21	17.6284	0.0471	bicyclo[4.4.1]undeca-1,3,5,7,9-pentaene
22	17.9811	0.0943	5-formyl-2,3,3',4'-tetramethoxystilbene
23	18.0829	0.5628	1,1-biphenyl, 3-methyl-
24	18.4906	0.3772	10,13-octadecadiynoic acid, methyl ester
25	18.5938	0.9107	naphthalene, 1,6,7-trimethyl-
26	18.8953	0.0691	9,10-secocholesta-5,7,10(19)-, (3ß,5z,7e)-
27	19.0027	0.1481	pregn-4-ene-3,20-dione, 16,17-epoxy-16-
28	19.1057	0.5541	10,13-octadecadiynoic acid, methyl ester
29	19.2153	0.2264	naphthalene, 1,6,7-trimethyl-
30	19.3184	0.7386	5-formyl-2,3,3',4'-tetramethoxystilbene
31	19.5231	0.2334	1,1'-biphenyl, 3-methyl-
32	19.6263	0.0784	octadecane, 3-ethyl-5-(2-ethylbutyl)-

33	19.9321	0.1053	5-formyl-2,3,3',4'-tetramethoxystilbene
34	20.0356	0.2527	10,13-octadecadiynoic acid, methyl ester
35	20.1391	0.1797	naphthalene, 1,3-dimethyl-
36	20.2438	0.5794	5,8,11-heptadecatriynoic acid, methyl ester
37	20.3476	0.9401	1,1'-biphenyl, 3-methyl-
38	20.4517	0.4392	phorbol 12,13-dihexanoate
39	20.5531	0.1544	9,10-secocholesta-5,7,10(19)-, (3ß,5z,7e)-
40	20.6554	0.8651	pregn-4-ene-3,20-dione, 16,17-epoxy-16-
41	20.7591	0.3806	5,8,11-heptadecatriynoic acid, methyl ester
42	20.8622	0.5339	benzene, 1,1',1",1'"-(1,6-hexanediylidene)tetrakis-
43	20.9174	0.5594	ferrioxamine
44	20.9702	0.2434	8h-azecino-8-one,5-octahydro-6-hydroxyethy-]-
45	21.0733	0.0522	1,1'-biphenyl, 3-methyl-
46	21.1797	0.0592	bicyclo[4.4.1]undeca-1,3,5,7,9-pentaene
47	21.2815	0.9314	cyclotrisiloxane, hexamethyl-
48	21.3841	0.1753	octadecane, 3-ethyl-5-(2-ethylbutyl)-
49	21.4866	1.7961	pregn-4-ene-3,20-dione, 16,17-epoxy-
50	21.5906	0.1135	10,13-octadecadiynoic acid, methyl ester
51	21.6467	2.5905	Fluorene
52	22.0997	0.1849	phorbol 12,13-dihexanoate
53	22.2107	0.1074	corynan-17-ol, 18,19-didehydro-10-methoxy-
54	22.6159	0.1327	octadecane, 3-ethyl-5-(2-ethylbutyl)-
55	22.7187	1.7961	5,8,11-heptadecatriynoic acid, methyl ester
56	22.8233	0.1135	biliverdin
57	22.9254	0.1905	1,1'-biphenyl, 3-methyl-
58	23.1311	0.1849	ferrioxamine
59	23.2365	0.1074	phorbol 12,13-dihexanoate
60	23.4419	0.1327	1,1'-biphenyl, 3-methyl-
61	23.6447	0.2189	cyclotrisiloxane, hexamethyl-
62	23.9467	0.2883	biliverdin
63	24.1514	0.1025	2,5-bis(1-naphthyl)-1,5-hexadiene
64	24.4599	0.0522	1,1'-biphenyl, 2-methyl-
65	24.6701	0.1291	dibenzofuran, 4-methyl-
66	25.0739	0.6164	curan-17-oic acid, 19-hydroxy-, methyl ester-
67	25.2812	20.3581	phenanthrene
68	25.4878	10.4107	anthracene
69	25.6894	0.1002	(2,3-diphenyl-aziridin-1-yl)-hept-2-ylidene)-amine
70	25.7989	0.5388	9h-fluorene, 2-methyl-
71	26.0158	0.301	morphinan-4,5-diol-6-one, 1-bromo-
72	26.4224	0.2528	coproporphyrin i
73	26.5366	0.2571	morphinan-4,5-diol-6-one, 1-bromo-
74	26.2001	0.0641	hexasiloxane, 1,1,3,3,5,5,7,7,9,9,11,11-dodecamethyl-
75	26.4834	0.1484	3,5-dihydroxy-3-methyl-pentanamide, n-benzhydryl-
76	26.6854	0.9534	carbazole

77	26.7903	0.2293	coproporphyrin ii
78	26.8934	0.9077	9,10-ethanoanthracene, 9,10-dihydro-11,12-diacetyl-
79	26.9529	0.2128	hexasiloxane, 1,1,3,3,5,5,7,7,9,9,11,11-dodecamethyl-
80	26.9761	0.4784	coproporphyrin iii
81	27.0106	0.6317	benzene, 1,1',1",1'"-(1,6-hexanediylidene)tetrakis-
82	27.1139	1.0596	3,5-dihydroxy-3-methyl-pentanamide, n-benzhydryl-
83	27.4198	1.6788	9,10-dihydro-anthracene
84	27.5233	0.0731	morphinan-4,5-diol-6-one, 1-bromo-
85	27.7268	0.0454	cyclopentadienyl-trichlorgermyl-dicarbonyl-molybdaen
86	28.1419	0.0376	1h-cyclopropa[l]phenanthrene,1a,9b-dihydro-
87	28.2521	0.3989	benzene, 1,1',1",1'"-(1,6-hexanediylidene)tetrakis-
88	28.4561	0.1472	4-acetyloxyimino-6,6-dimethyl-benzo[c]thiophene-
89	28.8632	0.2742	(2,3-diphenyl-aziridin-1-yl)-hept-2-ylidene)-amine
90	29.2699	0.6833	coproporphyrin ii
91	29.3717	0.2899	curan-17-oic acid, 19-hydroxy-, methyl ester-
92	29.2111	0.1071	hexasiloxane, 1,1,3,3,5,5,7,7,9,9,11,11-dodecamethyl-
93	29.4115	0.0979	1h-cyclopropa[l]phenanthrene,1a,9b-dihydro-
94	29.5196	0.1195	morphinan-4,5-diol-6-one, 1-bromo-
95	29.6267	0.1148	3-methyl-6,7-benzoisoquinoline
96	27.7331	0.2981	1,2,4,3,5-triselenadiborolane, 3,5-diethyl-
97	30.1317	0.9015	benzene, 1,1',1",1'"-(1,6-hexanediylidene)tetrakis-
98	30.3358	0.7413	1,2,4,3,5-triselenadiborolane, 3,5-diethyl-
99	30.4452	0.1727	1h-cyclopropa[l]phenanthrene,1a,9b-dihydro-
100	30.5443	0.7443	1,2,4,3,5-triselenadiborolane, 3,5-diethyl-
101	30.8463	0.9411	9,9'-biphenanthrene, octacosahydro-
102	31.2198	1.8992	pyrene
103	31.6233	0.9439	2-azatricyclononane-3-carboxylic acid, 4-phenyl-butyl-
104	32.0267	0.0781	cyclotrisiloxane, hexamethyl-
105	32.3419	0.3284	1,2,4,3,5-triselenadiborolane, 3,5-diethyl-

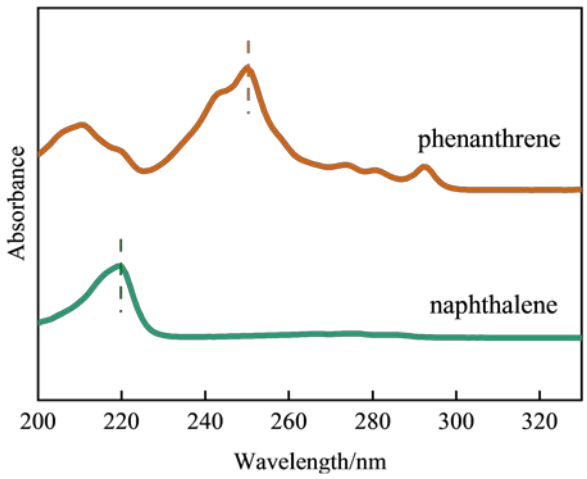

Figure S1. Ultraviolet-visible spectroscopy of naphthalene and phenanthrene.

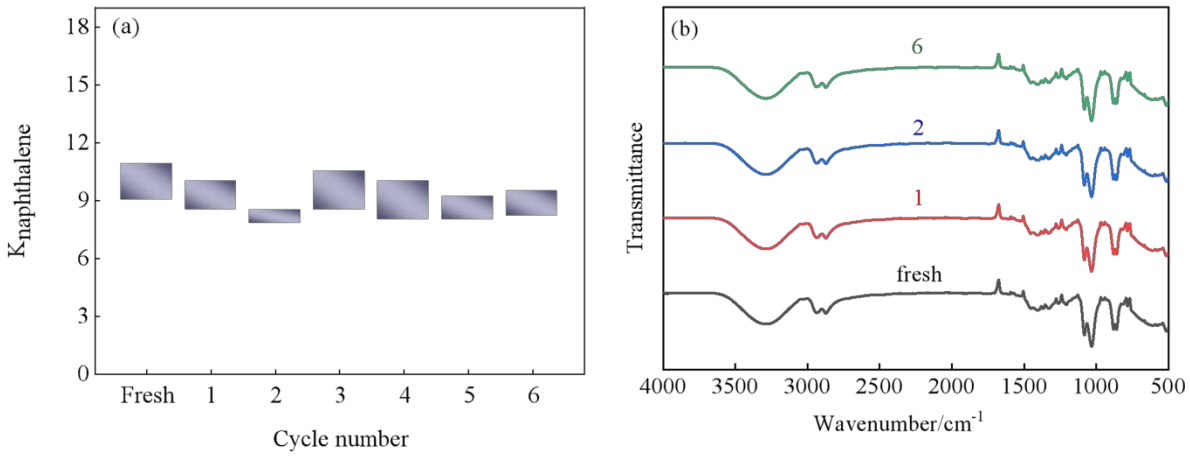

Figure S2. The reusability of the naphthalene-based solvent: (a) separation performance and (b) structural integrity.

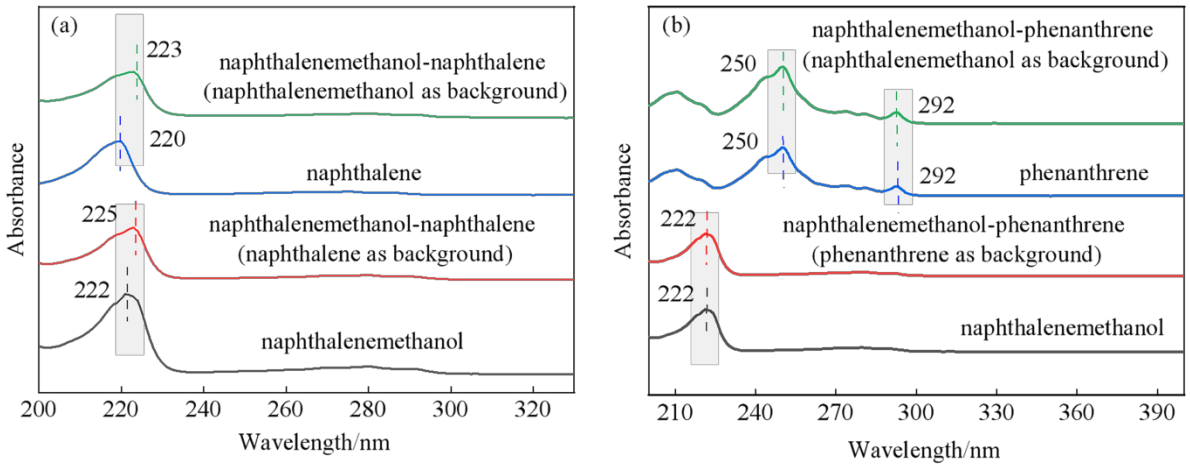

Figure S3. Ultraviolet-visible spectroscopy of (a) naphthalene, naphthalenemethanol, naphthalenemethanol-naphthalene and (b) phenanthrene, naphthalenemethanol, naphthalenemethanol-phenanthrene.

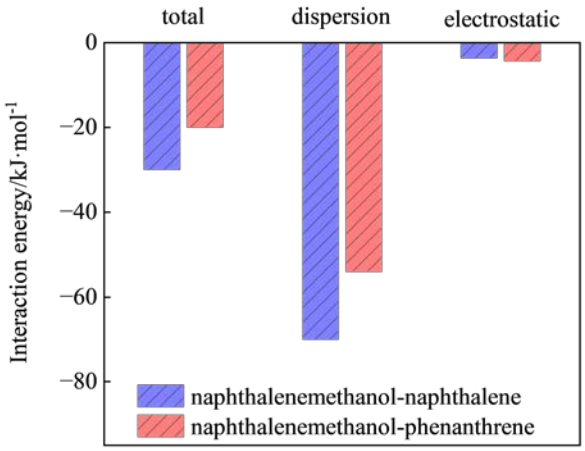

Figure S4. The total non-bonded interaction energy, dispersion and electrostatic interaction energy between naphthalenemethanol and naphthalene or phenanthrene

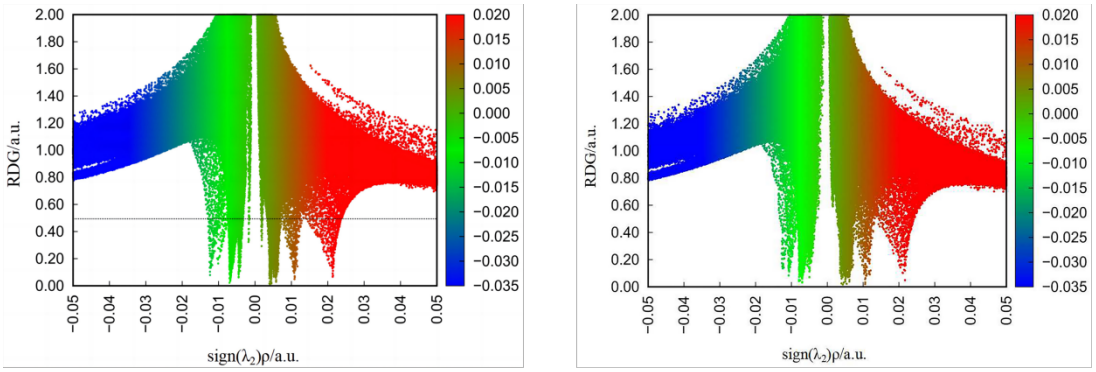

Figure S5. RDG color-filled scatter figures for (left) naphthalenemethanol-naphthalene and (right) naphthalenemethanol-phenanthrene.

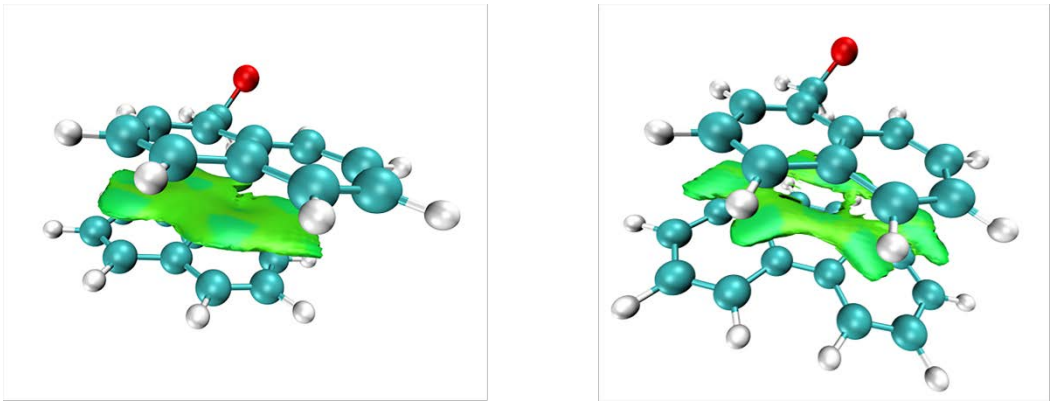

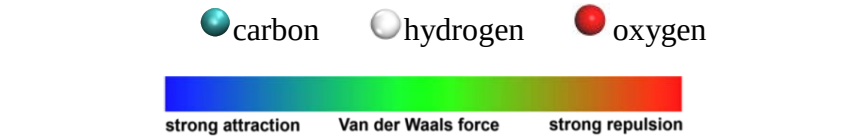

Figure S6. IGM analysis of naphthalenemethanol-naphthalene (left) and naphthalenemethanol -phenanthrene (right)

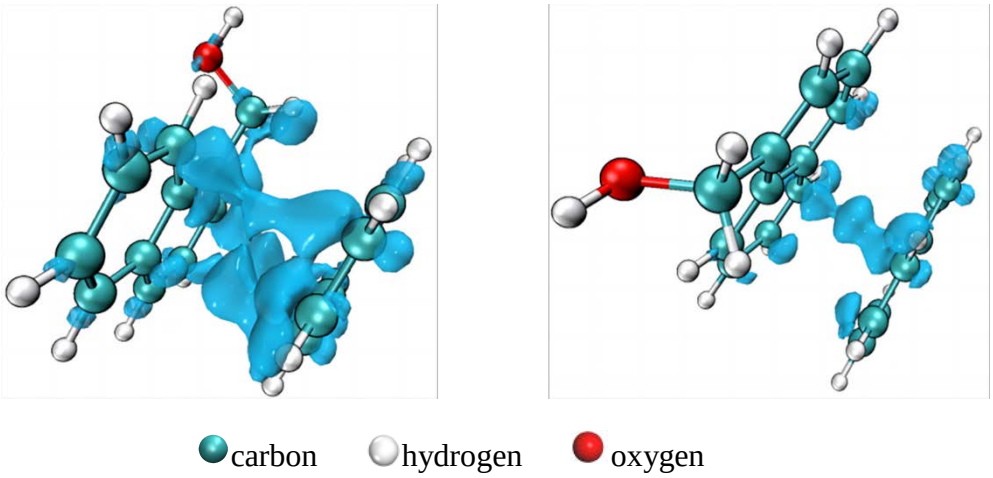

Figure S7. Electron density difference maps of naphthalenemethanol-naphthalene (left) and naphthalenemethanol-phenanthrene (right)

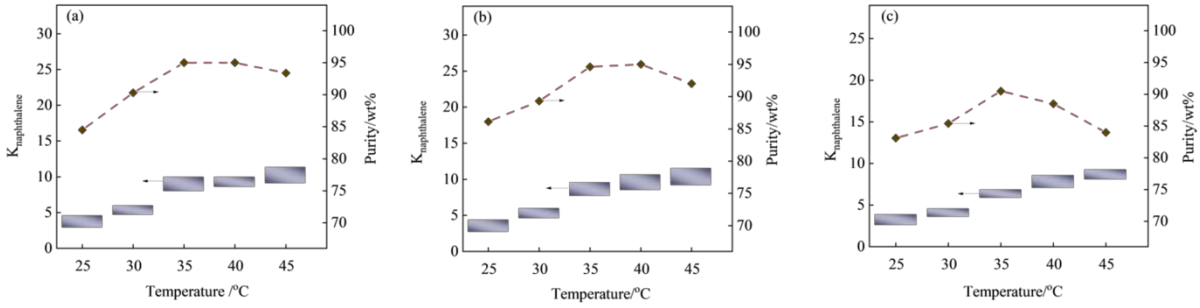

Figure S8 The effect of different separation systems on the separation performance of naphthalene methanol (a) naphthalene, phenanthrene and anthracene mixture; (b) naphthalene, phenanthrene, anthracene and fluorene (c) naphthalene, phenanthrene, anthracene, fluorene and carbazole mixture

References

1. Yi L, Feng J, Gauthier M, Li W Y. Effect of the addition of deep eutectic solvent to the anthracene separation. Journal of Molecular Liquids, 2021, 339: 116762
2. Frisch, M. J.; Trucks, G. W.; Schlegel, H. B.; Scuseria, G. E.; Robb, M. A.; heeseman, J. R.; Scalmani, G.; Barone, V.; Mennucci, B.; Petersson, G. A.; Nakatsuji, H.; Caricato, M.; Li, X.; Hratchian, H. P.; Izmaylov, A. F.; Bloino, J.; Zheng, G.; Sonnenberg, J. L.; Hada, M.; Ehara, M.; Toyota, K.; Fukuda, R.; Hasegawa, J.; Ishida, M.; Nakajima, T.; Honda, Y.; Kitao, O.; Nakai, H.; Vreven, T.; Montgomery, J. A., Jr.; Peralta, J. E.; Ogliaro, F.; Bearpark, M.; Heyd, J. J.; Brothers, E.; Kudin, K. N.; Staroverov, V. N.; Kobayashi, R.; Normand, J.; Raghavachari, K.; Rendell, A.; Burant, J. C.; Iyengar, S. S.; Tomasi, J.; Cossi, M.; Rega, N.; Millam, N. J.; Klene, M.; Knox, J. E.; Cross, J. B.; Bakken, V.; Adamo, C.; Jaramillo, J.; Gomperts, R.; Stratmann, R. E.; Yazyev, O.; Austin, A. J.; Cammi, R.; Pomelli, C.; Ochterski, J. W.; Martin, R. L.; Morokuma, K.; Zakrzewski, V. G.; Voth, G. A.; Salvador, P.; Dannenberg, J. J.; Dapprich, S.; Daniels, A. D.; Farkas, O.; Foresman, J. B.; Ortiz, J. V.; Cioslowski, J.; Fox, D. J. Gaussian 09; Gaussian, Inc., Wallingford, CT, 2009
3. Lu T, Liu Z, Chen Q. Comment on “18 and 12 – Member carbon rings (cyclo[n]carbons) – A density functional study”. Materials Science and Engineering: B, 2021, 273: 115425
4. Lu T, Chen Q. A simple method of identifying π orbitals for non-planar systems and a protocol of studying π electronic structure. Theoretical Chemistry Accounts, 2020, 139(2): 25
5. Johnson E R, Keinan S, Mori-Sánchez P, Contreras-García J, Cohen A J, Yang W. Revealing noncovalent interactions. Journal of the American Chemical Society, 2010, 132(18): 6498-6506
6. Lefebvre C, Rubez G, Khartabil H, Boisson J-C, Contreras-García J, Hénon E. Accurately extracting the signature of intermolecular interactions present in the NCI plot of the reduced density gradient versus electron density. Physical Chemistry Chemical Physics, 2017, 19(27): 17928-17936
7. Lu T, Chen Q. Independent gradient model based on Hirshfeld partition: A new method for visual study of interactions in chemical systems. Journal of Computational Chemistry, 2022, 43(8): 539-555
8. Lu T, Chen F. Multiwfn: A multifunctional wavefunction analyzer. Journal of Computational Chemistry, 2011, 33(5): 580-592
9. Humphrey W, Dalke A, Schulten K. VMD: Visual molecular dynamics. Journal of Molecular Graphics, 1996, 14(1): 33-38